Monthly Notices of the ROYAL ASTRONOMICAL SOCIETY

MNRAS **511,** 4147–4158 (2022)
Advance Access publication 2022 January 29

https://doi.org/10.1093/mnras/stac255

Kaniadakis-holographic dark energy: observational constraints and global dynamics

A. Hernández-Almada,[1★] Genly Leon,[2] Juan Magaña,[3] Miguel A. García-Aspeitia,[4,5,6] V. Motta,[7] Emmanuel N. Saridakis[8,9,10] and Kuralay Yesmakhanova[10,11]

[1]*Facultad de Ingeniería, Universidad Autónoma de Querétaro, Centro Universitario Cerro de las Campanas, 76010 Santiago de Querétaro, México*
[2]*Departamento de Matemáticas, Universidad Católica del Norte, Avda. Angamos 0610, Casilla 1280 Antofagasta, Chile*
[3]*Instituto de Astrofísica & Centro de Astro-Ingeniería, Pontificia Universidad Católica de Chile, Av. Vicuña Mackenna, 4860 Santiago, Chile*
[4]*Depto. de Física y Matemáticas, Universidad Iberoamericana Ciudad de México, Prolongación Paseo de la Reforma 880, México D. F. 01219, México*
[5]*Universidad Autónoma de Zacatecas, Calzada Solidaridad esquina con Paseo a la Bufa S/N C.P. 98060, Zacatecas, México*
[6]*Consejo Nacional de Ciencia y Tecnología, Av. Insurgentes Sur 1582. Colonia Crédito Constructor, Del. Benito Juárez C.P. 03940, Ciudad de México, México*
[7]*Instituto de Física y Astronomía, Facultad de Ciencias, Universidad de Valparaíso, Avda. Gran Bretaña 1111, Valparaíso, Chile*
[8]*Institute for Astronomy, Astrophysics, Space Applications and Remote Sensing, National Observatory of Athens, Lofos Nymfon, 11852 Athens, Greece*
[9]*CAS Key Laboratory for Researches in Galaxies and Cosmology, Department of Astronomy, University of Science and Technology of China, Hefei, Anhui 230026, P.R. China*
[10]*Ratbay Myrzakulov Eurasian International Centre for Theoretical Physics, Nur-Sultan 010009, Kazakhstan*
[11]*Ratbay Myrzakulov Eurasian International Centre for Theoretical Physics, Eurasian National University, Nur-Sultan Astana 010008, Kazakhstan*

Accepted 2022 January 25. Received 2022 January 25; in original form 2021 November 19

ABSTRACT

We investigate Kaniadakis-holographic dark energy by confronting it with observations. We perform a Markov Chain Monte Carlo analysis using cosmic chronometers, supernovae type Ia, and Baryon Acoustic Oscillations data. Concerning the Kaniadakis parameter, we find that it is constrained around zero, namely around the value in which Kaniadakis entropy recovers standard Bekenstein-Hawking one. Additionally, for the present matter density parameter $\Omega_m^{(0)}$, we obtain a value slightly smaller compared to ΛCDM scenario. Furthermore, we reconstruct the evolution of the Hubble, deceleration, and jerk parameters extracting the deceleration-acceleration transition redshift as $z_T = 0.86^{+0.21}_{-0.14}$. Finally, performing a detailed local and global dynamical system analysis, we find that the past attractor of the Universe is the matter-dominated solution, while the late-time stable solution is the dark-energy-dominated one.

Key words: cosmological parameters – dark energy – cosmology: theory.

1 INTRODUCTION

The acceleration of the Universe is one of the most elusive problems in modern cosmology. Since its discovery in the last decade of the twentieth century by Supernovae (SNIa) observations (Riess et al. 1998; Perlmutter et al. 1999), and its confirmation by the acoustic peaks of the cosmic microwave background radiation (Spergel et al. 2003), it has been a theoretical and observational challenge to construct a model that combines all of its characteristics. From a theoretical point of view, and assuming homogeneous and isotropic symmetries (cosmological principle), the need for a component with features able to reproduce the Universe acceleration is vital to obtain accurate values for the observable Universe age and size. Recently, the confidence in the detection of this acceleration at late times has been increased with precise observations of the large-scale structure (Nadathur et al. 2020).

The best candidate to explain the observed acceleration is the well-known cosmological constant (CC), interpreted under the assumption that quantum vacuum fluctuations generate the constant energy density observed and, with this, a late-time acceleration. However, when we apply the Quantum Field Theory to assess the energy density, the result is in total discrepancy with observations, giving rise to the so-called *fine-tuning problem* (Zel'dovich, Krasinski & Zeldovich 1968; Weinberg 1989). In addition, recent observations developed by the collaboration *Supernova H_0 for the Equation of State* (SH0ES; Riess et al. 2021) show a discrepancy for the obtained value of H_0 when compared to Planck observations based on the Λ Cold Dark Matter (ΛCDM) model (Aghanim et al.). This generates a tension of 4.2σ between the mentioned experiments, bringing a new crisis and the need for new ways to tackle the problem (Di Valentino et al. 2021), as long as this discrepancy is not related to unknown systematic errors affecting the measurements (Shajib et al. 2020; Birrer & Treu 2021; Efstathiou 2021; Freedman 2021; Shah, Lemos & Lahav 2021). In this vein the community has been proposing other alternatives to address the problem of the Universe acceleration. In general, there are two main directions that one could follow. The first is to maintain general relativity and introduce new peculiar forms of matter, such as scalar fields (Copeland, Sami & Tsujikawa 2006; Cai et al. 2010; Motta et al. 2021), Chaplygin gas (Chaplygin 1904;

★ E-mail: ahalmada@uaq.mx

Villanueva 2015; Hernández-Almada et al. 2019), viscous fluids (Cruz, Cruz & Lepe 2017; Cruz, Hernández-Almada & Cornejo-Pérez 2019; Hernández-Almada 2019; Hernández-Almada et al. 2020a), etc, collectively known as the dark-energy sector. The second way is to construct modified gravitational theories (Capozziello & De Laurentis 2011; Saridakis et al. 2021) such as braneworlds models (Maartens & Koyama 2010; García-Aspeitia et al. 2017; Garcia-Aspeitia et al. 2018), emergent gravity (García-Aspeitia et al. 2019, 2021; Li & Shafieloo 2019; Pan et al. 2019; Hernández-Almada et al. 2020b; Li & Shafieloo 2020), Einstein-Gauss-Bonet (Glavan & Lin 2020; García-Aspeitia & Hernández-Almada 2021), thermodynamical models (Leon et al. 2021; Saridakis & Basilakos 2021), torsional gravity (Cai et al. 2016), $f(R)$ theories (Dainotti et al. 2021), etc.

On the other hand, there is an increasing interest in dark energy alternative models with the holographic principle. This is inspired by the relation between entropy and the area of a black hole. It states that the observable degree of freedom of a physical system in a volume can be encoded in a lower-dimensional description on its boundary ('t Hooft 1993; Susskind 1995). The holographic principle imposes a connection between the infrared cut-off, related to large scale of the Universe, with the ultraviolet one, related to the vacuum energy. Application of the holographic principle to the Universe horizon gives rise to a vacuum energy of holographic origin, namely holographic dark energy (Li 2004; Wang, Wang & Li 2017). Holographic dark energy proves to lead to interesting phenomenology and, thus, it has been studied in detailed (Horvat 2004; Li 2004; Pavon & Zimdahl 2005; Wang, Gong & Abdalla 2005; Kim, Lee & Myung 2006; Nojiri & Odintsov 2006; Setare & Saridakis 2009, 2008; Wang et al. 2017), confronted to observations (Zhang & Wu 2005; Feng et al. 2007; Li et al. 2009; Zhang 2009; Lu et al. 2010; Micheletti 2010) and extended to various frameworks (Gong 2004; Cai 2007; Saridakis 2008a, b; Setare & Vagenas 2008; Suwa & Nihei 2010; Bouhmadi-Lopez, Errahmani & Ouali 2011; Khurshudyan et al. 2014; Nojiri & Odintsov 2017; Saridakis 2018, 2020; Saridakis et al. 2018; Dabrowski & Salzano 2020; Kritpetch, Muhammad & Gumjudpai 2020; Bhattacharjee 2021; da Silva & Silva 2021; Colgáin & Sheikh-Jabbari 2021; Huang et al. 2021; Lin 2021; Mamon, Paliathanasis & Saha 2021; Nojiri, Odintsov & Paul 2021; Shekh 2021).

Recently, an extension of the holographic dark energy scenario was constructed in (Drepanou et al. 2021), based on Kaniadakis entropy. The latter is an extended entropy arising from the relativistic extension of standard statistical theory, quantified by one new parameter (Kaniadakis 2002, 2005). In the case where this Kaniadakis parameter becomes zero, i.e. when Kaniadakis entropy becomes the standard Bekenstein-Hawking entropy, Kaniadakis-holographic dark energy recovers standard-holographic dark energy, however, in the general case, it exhibits a range of behaviours with interesting cosmological implications.

In this work, we investigate Kaniadakis-holographic dark energy, in order to tackle the late-time universe acceleration problem. The outline of the paper is as follows. In Section 2 the mathematical background of the model is considered, presenting the master equations. Section 3 presents the observational confrontation analysis that includes three data samples and the results from the corresponding constraints. Section 4 is dedicated to the dynamical system investigation and the stability analysis. Finally, in Section 5 we give a brief summary and a discussion of the results. Throughout the manuscript, we use natural units where $\tilde{c} = \hbar = k_B = 1$ (unless stated otherwise).

2 KANIADAKIS-HOLOGRAPHIC DARK ENERGY

In this section we briefly review Kaniadakis-holographic dark energy, and we elaborate the corresponding equations in order to bring them to a form suitable for observational confrontation. The essence of holographic dark energy is the inequality $\rho_{DE} L^4 \leq S$, with ρ_{DE} being the holographic dark energy density, L the largest distance (typically a horizon), and S the entropy expression in the case of a black hole with a horizon L (Li 2004; Wang et al. 2017). In the standard application using Bekenstein-Hawking entropy $S_{BH} \propto A/(4G) = \pi L^2/G$, where A is the area and G the Newton's constant, one obtains standard-holographic dark energy, i.e. $\rho_{DE} = 3c^2 M_p^2 L^{-2}$, where $M_p^2 = (8\pi G)^{-1}$ is the Planck mass and c is the model parameter arising from the saturation of the above inequality.

On the other hand, one can construct the one-parameter generalization of the classical entropy, namely Kaniadakis entropy $S_K = -k_{_B} \sum_i n_i \ln_{\{K\}} n_i$ (Kaniadakis 2002, 2005), where $k_{_B}$ is the Boltzmann constant and with $\ln_{\{K\}} x = (x^K - x^{-K})/2K$. This is characterized by the dimensionless parameter $-1 < K < 1$, which accounts for the relativistic deviations from standard statistical mechanics, and in the limit $K \to 0$, it recovers standard entropy. Kaniadakis entropy can be re-expressed as (Abreu et al. 2016, 2018; Abreu & Ananias Neto 2021)

$$S_K = -k_{_B} \sum_{i=1}^{W} \frac{P_i^{1+K} - P_i^{1-K}}{2K}, \tag{1}$$

where P_i is the probability of a specific microstate of the system and W is the total number of possible configurations. Applied in the black hole framework, it results into (Moradpour, Ziaie & Kord Zangeneh 2020; Drepanou et al. 2021; Lymperis, Basilakos & Saridakis 2021)

$$S_K = \frac{1}{K} \sinh(K S_{BH}), \tag{2}$$

which gives standard Bekenstein-Hawking entropy in the limit $K \to 0$. Finally, since any deviations from standard thermodynamics are expected to be small, one can approximate (2) for $K \ll 1$, acquiring (Drepanou et al. 2021)

$$S_K = S_{BH} + \frac{K^2}{6} S_{BH}^3 + \mathcal{O}(K^4). \tag{3}$$

In order to analyse the dynamics of the universe, we consider the homogeneous and isotropic cosmology based on the Friedmann-Lemaître-Robertson-Walker line element $\mathrm{d}s^2 = -\mathrm{d}t^2 + a(t)(\mathrm{d}r^2 + r^2\mathrm{d}\Omega^2)$, where $\mathrm{d}\Omega^2 \equiv \mathrm{d}\theta^2 + \sin^2\theta \mathrm{d}\varphi^2$, $a(t)$ is the scale factor and we consider null spatial curvature $k = 0$. Furthermore, as usual we use L as the future event horizon $R_h \equiv a \int_t^\infty \frac{1}{a(s)} \mathrm{d}s$. Inserting these into the above formulation, and using Kaniadakis entropy instead of Bekenstein-Hawking one, we extract the energy density of Kaniadakis-holographic dark energy as (Drepanou et al. 2021)

$$\rho_{DE} = \frac{3c^2 M_p^2}{R_h^2} + K^2 M_p^6 R_h^2, \tag{4}$$

with $c > 0$ and K being the two parameters of the model. Hence, we can write the Friedmann and Raychaudhuri equations as

$$H^2 = \frac{1}{3M_p^2}(\rho_m + \rho_{DE}), \tag{5}$$

$$\dot{H} = -\frac{1}{2M_p^2}(\rho_m + p_m + \rho_{DE} + p_{DE}), \tag{6}$$

where $H \equiv \dot{a}/a$ is the Hubble parameter, ρ_m and p_m are the energy density and pressure of matter perfect fluid, while the matter conservation leads to dark energy conservation and, in turn, to the dark energy pressure

$$p_{DE} = -\frac{2c^2 M_p^2}{R_h^3 H} - \frac{c^2 M_p^2}{R_h^2} + K^2 M_p^6 \left[\frac{2R_h}{3H} - \frac{5}{3}R_h^2\right]. \quad (7)$$

The combination of Raychaudhuri equations (6, 4, and 7) give

$$\dot{H} = \frac{c^2}{R_h^3 H} + \frac{c^2(3w_m+1)}{2R_h^2} - \frac{3}{2}(w_m+1)H^2 - K^2 M_p^4 \left[\frac{R_h}{3H} - \frac{1}{6}R_h^2(3w_m+5)\right], \quad (8)$$

where $w_m \equiv p_m/\rho_m$ is the equation-of-state parameter for matter, considered from now on as dust ($w_m = 0$). From this expression we can construct the deceleration and jerk parameters, which give us information about the transition to an accelerated Universe. Thus, using the definition of R_h, we obtain that the energy density is

$$\rho_{DE} = \frac{3c^2 M_p^2}{a^2\left(\int_t^\infty \frac{1}{a(s)}\,\mathrm{d}s\right)^2} + K^2 M_p^6 a^2 \left(\int_t^\infty \frac{1}{a(s)}\,\mathrm{d}s\right)^2, \quad (9)$$

and the pressure

$$p_{DE} = -\frac{2c^2 M_p^2}{a^3 H\left(\int_t^\infty \frac{1}{a(s)}\,\mathrm{d}s\right)^3} - \frac{c^2 M_p^2}{a^2\left(\int_t^\infty \frac{1}{a(s)}\,\mathrm{d}s\right)^2} + K^2 M_p^6 \left[\frac{2a\left(\int_t^\infty \frac{1}{a(s)}\,\mathrm{d}s\right)}{3H} - \frac{5}{3}a^2\left(\int_t^\infty \frac{1}{a(s)}\,\mathrm{d}s\right)^2\right]. \quad (10)$$

Moreover, the fractional energy density of DE is defined as

$$\Omega_{DE} := \frac{\rho_{DE}}{3M_p^2 H^2} = \frac{K^2 M_p^6 a^4 \left(\int_t^\infty \frac{1}{a(s)}\,\mathrm{d}s\right)^4 + 3c^2 M_p^2}{3M_p^2 a^2 H^2 \left(\int_t^\infty \frac{1}{a(s)}\,\mathrm{d}s\right)^2}. \quad (11)$$

From definition (11), we have four branches for

$$\mathcal{I}(t) := \int_t^\infty a(s)^{-1}\,\mathrm{d}s, \quad (12)$$

which give four possible expressions for the particle horizon

$$R_{h1,2}(t) = \mp \frac{\left[3H^2\Omega_{DE} - \sqrt{9H^4\Omega_{DE}^2 - 12c^2K^2M_p^4}\right]^{1/2}}{\sqrt{2}|K|M_p^2}, \quad (13)$$

$$R_{h3,4}(t) = \mp \frac{\left[3H^2\Omega_{DE} + \sqrt{9H^4\Omega_{DE}^2 - 12c^2K^2M_p^4}\right]^{1/2}}{\sqrt{2}|K|M_p^2}. \quad (14)$$

$R_{h1}(t)$ and $R_{h3}(t)$ are both discarded since they lead to negative particle horizon. To decide between the choices $R_{h2}(t)$ and $R_{h4}(t)$, which are both non negative, we calculate the limit $K \to 0$ and obtain

$$\lim_{K\to 0} R_{h2} = \frac{c}{H\sqrt{\Omega_{DE}}}, \quad \lim_{K\to 0} R_{h4} = \infty. \quad (15)$$

That is, $R_{h2}(t)$ defined by (13) is the only physical solution.

We proceed by introducing the usual dimensionless variable

$$E \equiv \frac{H}{H_0}, \quad (16)$$

where H_0 is the Hubble constant at present time and, for convenience, we define the dimensionless constant $\beta \equiv \frac{KM_p^2}{H_0^2}$.

Differentiating (11) and (16), and using the Friedmann equations, we obtain the master equations

$$\Omega_{DE}' = (1-\Omega_{DE})\left[3(w_m+1)\Omega_{DE} + 2\mathcal{X}\right], \quad (17)$$

$$E' = E\left[-\frac{3}{2}(w_m+1)(1-\Omega_{DE}) + \mathcal{X}\right], \quad (18)$$

where

$$\mathcal{X} \equiv \frac{1}{E^3}\left[\frac{2\beta^2E^4\Omega_{DE}^2 - 8\beta^4c^2/3}{3E^2\Omega_{DE} - \sqrt{9E^4\Omega_{DE}^2 - 12\beta^2c^2}}\right]^{1/2} - \frac{1}{E^2}\left[E^4\Omega_{DE}^2 - 4\beta^2c^2/3\right]^{1/2}. \quad (19)$$

We use initial conditions $\Omega_{DE}(0) \equiv \Omega_{DE}^{(0)} = 1 - \Omega_m^{(0)}$, $E(0) = 1$, where primes denote derivatives with respect to e-foldings number $N = \ln(a/a_0)$, and $N = 0$ marks the current time (from now on, the index '0' marks the value of a quantity at present). The physical region of the phase space is

$$3E^4\Omega_{DE}^2 - 4\beta^2c^2 \geq 0. \quad (20)$$

Notice that $\mathcal{X} \to \frac{\Omega_{DE}^{3/2}}{c} - \Omega_{DE}$ as $\beta \to 0$.

From the matter conservation equation, we arrive at

$$\rho_m'(N) = -3(1+w_m)\rho_m, \quad \rho_m(0) = 3M_p^2H_0^2\Omega_m^{(0)}, \quad (21)$$

and, therefore, we have $\rho_m(N) = 3H_0^2M_p^2\Omega_m^{(0)}e^{-3N(w_m+1)}$ which then leads to

$$\Omega_{DE}(N) = 1 - \Omega_m(N) = 1 - \frac{\Omega_m^{(0)}e^{-3N(w_m+1)}}{E^2}. \quad (22)$$

Defining $Z = E^2$, we obtain the equation

$$Z' = -3(w_m+1)\Omega_m^{(0)}e^{-3N(w_m+1)} + 2\mathcal{X}Z, \quad Z(0) = 1, \quad (23)$$

where

$$\mathcal{X}Z = -\left[\left(\Omega_m^{(0)}e^{-3N(w_m+1)} - Z\right)^2 - \frac{4\beta^2c^2}{3}\right]^{1/2} + \left[\frac{2\beta^2\left(Z - \Omega_m^{(0)}e^{-3N(w_m+1)}\right)^2 - \frac{8\beta^4c^2}{3}}{3Z^2 - 3Z\Omega_m^{(0)}e^{-3N(w_m+1)} - Z\sqrt{9\left(Z - \Omega_m^{(0)}e^{-3N(w_m+1)}\right)^2 - 12\beta^2c^2}}\right]^{1/2}. \quad (24)$$

Thus, the evolution of $E^2(z)$ can be obtained by substituting (24) into (23). More precisely, substituting (24) into (23), integrating, and imposing the initial condition $Z(0) = 1$, gives $E^2(N)$. In order to express it as $E^2(z)$, we use the relation $N = \ln(a/a_0) = -\ln(1+z)$, which is a relation between the e-folding (N), the scale factor (a), and the redshift (z).

Additionally, we can now write the deceleration parameter $q(z)$, and a cosmographic parameter that is related to the third-order derivative of the scale factor, i.e. the cosmographic jerk parameter $j(z)$, which are given by the formulas

$$q := -1 - \frac{E'}{E}, \quad (25)$$

$$j := q(2q+1) - q', \quad (26)$$

where $j = 1$ corresponds to the case of a CC.

Hence, equation (25) becomes

$$q = -1 + \frac{3}{2}(w_m+1)(1-\Omega_{DE}) - \mathcal{X}, \quad (27)$$

with $\mathcal{X}$ defined by (19). j is found by direct evaluation of (26). We have mentioned before that taking the limit $\beta \to 0$ in (17) and

(18), and neglecting error terms $O(\beta^2)$, we acquire the approximated differential equations

$$\Omega'_{DE} = \frac{\Omega_{DE}(1-\Omega_{DE})\left(3w_m c + c + 2\sqrt{\Omega_{DE}}\right)}{c}, \tag{28}$$

$$E' = \frac{E\left\{2\Omega_{DE}^{3/2} + c[3w_m(\Omega_{DE}-1) + \Omega_{DE} - 3]\right\}}{2c}. \tag{29}$$

Equations (28) and (29) characterize standard holographic cosmology. Imposing the conditions

$$E(\Omega_{DE}^{(0)}) = 1, \quad \ln\left(\frac{a}{a_0}\right)\Big|_{\Omega_{DE}^{(0)}} = 0, \tag{30}$$

we obtain the implicit solutions

$$E = \left(\frac{\Omega_{DE}}{\Omega_{DE}^{(0)}}\right)^{-\frac{3(w_m+1)}{6w_m+2}} \left(\frac{1-\sqrt{\Omega_{DE}}}{1-\sqrt{\Omega_{DE}^{(0)}}}\right)^{\frac{c-1}{3cw_m+c+2}} \times \left(\frac{\sqrt{\Omega_{DE}}+1}{\sqrt{\Omega_{DE}^{(0)}}+1}\right)^{\frac{c+1}{3cw_m+c-2}} \times \left(\frac{3cw_m + c + 2\sqrt{\Omega_{DE}}}{3cw_m + c + 2\sqrt{\Omega_{DE}^{(0)}}}\right)^{-\frac{12(w_m+1)}{(3w_m+1)\left((3cw_m+c)^2-4\right)}}, \tag{31}$$

and

$$(1+z)^{-1} := \left(\frac{a}{a_0}\right) = \left(\frac{\Omega_{DE}}{\Omega_{DE}^{(0)}}\right)^{\frac{1}{3w_m+1}} \left(\frac{1-\sqrt{\Omega_{DE}}}{1-\sqrt{\Omega_{DE}^{(0)}}}\right)^{-\frac{c}{3cw_m+c+2}} \times \left(\frac{\sqrt{\Omega_{DE}}+1}{\sqrt{\Omega_{DE}^{(0)}}+1}\right)^{-\frac{c}{3cw_m+c-2}} \times \left(\frac{3cw_m + c + 2\sqrt{\Omega_{DE}}}{3cw_m + c + 2\sqrt{\Omega_{DE}^{(0)}}}\right)^{\frac{8}{(3w_m+1)\left((3cw_m+c)^2-4\right)}}. \tag{32}$$

Lastly, expanding around $\beta = 0$ and $\Omega_{DE} = 1$ and removing second-order terms, the deceleration parameter (25) and the cosmographic jerk parameter (26; in the dark-energy dominated epoch) are given by

$$q = -\frac{1}{c} + \frac{(1-\Omega_{DE})(3cw_m + c + 3)}{2c}, \tag{33}$$

$$j = \frac{2-c}{c^2} + \frac{(1-\Omega_{DE})(3cw_m + c + 3)[c(3w_m+2) - 2]}{2c^2}. \tag{34}$$

Furthermore, expanding around $\beta = 0$ and $\Omega_{DE} = 0$ and removing second-order terms, the deceleration parameter (25) and the cosmographic jerk parameter (26; in the matter-dominated epoch) are given by

$$q = \frac{1}{2}(3w_m + 1)(1-\Omega_{DE}), \tag{35}$$

$$j = \frac{1}{2}[9w_m(w_m+1) + 2](1-\Omega_{DE}). \tag{36}$$

3 OBSERVATIONAL ANALYSIS

One of the goals of this work is to provide observational bounds on the parameter of Kaniadakis entropy K or, more conveniently β; however, we are also interested in the behaviour of all cosmological parameters, namely on the vector $\boldsymbol{\Theta} = \{h, \Omega_m^{(0)}, \beta, c\}$. For the parameter estimation, we use the recent measurements of the observational Hubble data, as well as data from type Ia SNIa and baryon acoustic oscillations (BAOs) observations. In what follows, we first briefly introduce these data sets and the Bayesian methodology, and then we apply it in the scenario of Kaniadakis-holographic dark energy, providing the resulting observational constraints.

3.1 Data and methodology

3.1.1 Cosmic chronometer data

The Hubble parameter $H(z)$ describes the expansion rate of the Universe as a function of redshift z. Currently, this parameter can be estimated from baryon acoustic oscillations measurements and differential age in passive galaxies (dubbed as cosmic chronometers). While the former could be biased due to the assumption of a fiducial cosmology, the samples from cosmic chronometers are independent from the underlying cosmological model. Thus, in this work we only consider the 31 points from cosmic chronometer sample presented in Moresco et al. (2016) and Magaña et al. (2018) in the redshift range $0.07 < z < 1.965$. We assume a Gaussian likelihood function for this observation as $\mathcal{L}_{\rm CC} \propto \exp{(-\chi^2_{\rm CC}/2)}$, where the figure-of-merit is

$$\chi^2_{\rm CC} = \sum_i^{31} \left[\frac{H_{\rm mod}(\boldsymbol{\Theta}, z_i) - H_{\rm dat}(z_i)}{\sigma^i_{\rm dat}}\right]^2, \tag{37}$$

where $H_{\rm dat}(z_i)$ and σ^i_{obs} are the measured Hubble parameter and its observational uncertainty at the redshift z_i, respectively. The predicted Hubble parameter by the Kaniadakis-holographic dark energy is denoted by $H_{\rm mod}(\boldsymbol{\Theta})$, and it can be obtained by solving the system of equations (17–19).

3.1.2 Pantheon SNIa sample

Since the discovery of the late cosmic acceleration with the observations of high-redshift type Ia SNIa by Riess et al. (1998) and Perlmutter et al. (1999), the observation of these distant objects is a crucial test to determine if a cosmological scenario is a viable candidate for the description of the late-time Universe. The probe consists of confronting the observed luminosity distance (or distance module) of SNIa with the theoretical prediction of any model. Up to now, the Pantheon sample (Scolnic et al. 2018) is the largest collection of high-redshift SNIa, with 1048 data points with measured redshifts in the range $0.001 < z < 2.3$. The authors also provide a binned sample containing 40 points of binned distances $\mu_{\rm dat,\,bin}$ in the redshift range $0.014 < z < 1.61$. In this work, we use the binned set and we consider a Gaussian likelihood $\mathcal{L}_{SNIa} \propto \exp{(-\chi^2_{SNIa}/2)}$. By marginalizing the nuisance parameters, the figure-of-merit function χ^2_{SNIa} is given by

$$\chi^2_{SNIa} = a + \log\left(\frac{e}{2\pi}\right) - \frac{b^2}{e}, \tag{38}$$

where $a = \Delta\tilde{\mu}^T \cdot \boldsymbol{C}_P^{-1} \cdot \Delta\tilde{\mu}$, $b = \Delta\tilde{\mu}^T \cdot \boldsymbol{C}_P^{-1} \cdot \Delta\mathbf{1}$, $e = \Delta\mathbf{1}^T \cdot \boldsymbol{C}_P^{-1} \cdot \Delta\mathbf{1}$, and $\Delta\tilde{\mu}$ is the vector of residuals between the model distance modulus and the observed (binned) one. The covariance matrix $\boldsymbol{C_P}$ takes into account systematic and statistical uncertainties (Scolnic et al. 2018). Moreover, the theoretical counterpart of the distance modulus for any cosmological model is given by $\mu_{\rm mod}(\boldsymbol{\Theta}, z) = 5\log_{10}{(d_{\rm L}(\boldsymbol{\Theta}, z)/10\,{\rm pc})}$, where $d_{\rm L}$ is the luminosity distance given by

$$d_{\rm L}(\boldsymbol{\Theta}, z) = \frac{\tilde{c}}{H_0}(1+z)\int_0^z \frac{{\rm d}z'}{E(z')}, \tag{39}$$

where $\tilde{c}$ is the light speed.

3.1.3 Baryon acoustic oscillations

BAOs are fluctuation patterns in the matter density field as a result of internal interactions in the hot primordial plasma during the pre-recombination stage. Based on luminous red galaxies, a sample of 15 transversal BAO scale measurements within the redshift $0.110 < z < 2.225$ were collected by Nunes et al. (2020). Assuming a Gaussian likelihood, $\mathcal{L}_{\rm BAO} \propto \exp{(-\chi^2_{\rm BAO}/2)}$, we build the figure-of-merit function as

$$\chi^2_{\rm BAO} = \sum_{i=1}^{15}\left[\frac{\theta^i_{\rm dat} - \theta_{\rm mod}(\Theta, z_i)}{\sigma_{\theta^i_{\rm dat}}}\right]^2, \tag{40}$$

where $\theta^i_{\rm dat} \pm \sigma_{\theta^i_{\rm dat}}$ is the BAO angular scale and its uncertainty at 68 per cent measured at z_i. The theoretical BAO angular scale counterpart, denoted as $\theta_{\rm mod}$, is estimated by

$$\theta_{\rm mod}(z) = \frac{r_{\rm drag}}{(1+z)D_{\rm A}(z)}, \tag{41}$$

where $D_{\rm A} = d_{\rm L}(z)/(1+z)^2$ is the angular diameter distance at z, which depends on the dimensionless luminosity distance $d_{\rm L}(z)$, and $r_{\rm drag}$ is the sound horizon at the baryon drag epoch, considered to be $r_{\rm drag} = 137.7 \pm 3.6$ Mpc (Aylor et al. 2019).

3.1.4 Bayesian analysis

A Bayesian statistical analysis based on Markov Chain Monte Carlo (MCMC) algorithm is performed to bound the free parameters of the Kaniadakis-holographic dark energy. The MCMC approach is implemented through the EMCEE PYTHON module (Foreman-Mackey et al. 2013) in which we generate 1000 chains with 250 steps, each one after a burn-in phase. The latter is stopped when the chains have converged based on the auto-correlation time criteria. Thus, the inference of the parameter space is obtained by minimizing a Gaussian log-likelihood, $-2\,\ln(\mathcal{L}_{\rm data}) \propto \chi^2_{\rm data}$, considering flat priors in the intervals: $h \in [0.2, 1]$, $\Omega_m^{(0)} \in [0, 1]$, $\beta \in [-1, 1]$, $c \in [0, 2]$ for each data set. Additionally, a combined analysis is performed by assuming no correlation between the data sets, hence the figure of merit is

$$\chi^2_{\rm Joint} = \chi^2_{\rm CC} + \chi^2_{\rm SNIa} + \chi^2_{\rm BAO}, \tag{42}$$

namely, the sum of the χ^2 corresponding to each sample as previously defined.

3.2 Results from observational constraints

We perform the full confrontation described above for the scenario of Kaniadakis-holographic dark energy, and in Fig. 1 we present the 2D parameter likelihood contours at 68 per cent (1σ) and 99.7 per cent (3σ) confidence level (CL) respectively, alongside the corresponding 1D posterior distribution of the parameters. Additionally, Table 1 shows the mean values of the parameters and their uncertainties at 1σ.

In order to statistically compare these results with ΛCDM cosmology, we apply the corrected Akaike information criterion (AICc; Akaike 1974; Sugiura 1978; Hurvich & Tsai 1989) and

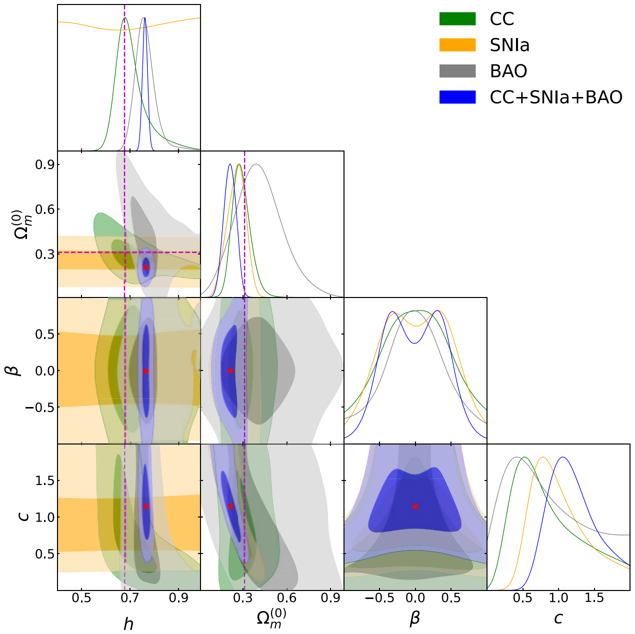

Figure 1. 2D likelihood contours at 68 per cent and 99.7 per cent CL, alongside the corresponding 1D posterior distribution of the free parameters, in Kaniadakis-holographic dark energy case. The stars denote the mean values using the joint analysis, and the dashed lines represent the best-fitting values for ΛCDM cosmology (Aghanim et al. 2020).

the Bayesian information criterion (BIC; Schwarz 1978). They give a penalty according to size of data sample (N) and the number of degrees of freedom (k) defined as AICc $= \chi^2_{min} + 2k + (2k^2 + 2k)/(N - k - 1)$ and BIC $= \chi^2_{min} + k\log(N)$, respectively, where χ^2_{min} is the minimum value of the χ^2. Thus, a model with lower values of AICc and BIC is preferred by the data. According to the difference between a given model and the reference one, denoted as ΔAICc, one has the following: if ΔAICc < 4, both models are supported by the data equally, i.e they are statistically equivalent. If $4 <$ ΔAICc < 10, the data still support the given model but less than the preferred one. If ΔAICc > 10, it indicates that the data do not support the given model. Similarly, the difference between a candidate model and the reference model, denoted as ΔBIC, is interpreted in this way: if ΔBIC < 2, there is no evidence against the candidate model, if $2 <$ ΔBIC < 6, there is modest evidence against the candidate model, if $6 <$ ΔBIC < 10, there is strong evidence against the candidate model, and ΔBIC > 10 gives the strongest evidence against it. Hence, we have performed the above comparison, taking ΛCDM scenario as the reference model, and we display the results in the last two columns of Table 1.

A first observation is that the Kaniadakis parameter β is constrained around 0 as expected, namely around the value in which Kaniadakis entropy recovers the standard Bekenstein-Hawking one. A second observation is that the scenario at hand gives a slightly smaller value for $\Omega_m^{(0)}$ comparing to ΛCDM cosmology, however it estimates a higher value for the present Hubble constant h, closer to its direct measurements through long-period Cepheids. In particular, it is consistent within 1σ with the value reported by Riess et al. (2019) and it exhibits a deviation of 4.18σ from the one obtained by Planck Aghanim et al. (2020). On the other hand, based on our mean value of $c = 1.151^{+0.401}_{-0.287}$ it is interesting that we do not observe a turning point in the $H(z)$ reconstruction shown in Fig. 2, a feature from which the usual holographic dark energy suffers when $c < 1$ (Colgáin & Sheikh-

Table 1. Mean values of various parameters and their 68 per cent CL uncertainties for Kaniadakis-holographic dark energy. The quantities ΔAICc (ΔBIC) are the differences with respect to ΛCDM paradigm.

Sample	χ^2	h	$\Omega_m^{(0)}$	β	c	ΔAICc	ΔBIC
CC	14.69	$0.690^{+0.072}_{-0.043}$	$0.284^{+0.066}_{-0.055}$	$0.012^{+0.486}_{-0.489}$	$0.729^{+0.665}_{-0.350}$	5.2	7.0
SNIa	48.52	$0.597^{+0.279}_{-0.271}$	$0.259^{+0.059}_{-0.069}$	$0.013^{+0.480}_{-0.482}$	$0.932^{+0.492}_{-0.302}$	5.1	7.5
BAO	13.01	$0.758^{+0.041}_{-0.035}$	$0.403^{+0.167}_{-0.151}$	$-0.006^{+0.433}_{-0.418}$	$0.756^{+0.759}_{-0.463}$	8.2	5.6
CC+SNIa + BAO	98.07	$0.761^{+0.011}_{-0.010}$	$0.211^{+0.043}_{-0.044}$	$-0.003^{+0.412}_{-0.420}$	$1.151^{+0.401}_{-0.287}$	21.7	26.1

Jabbari 2021). Hence, we deduce that Kaniadakis-holographic dark energy can also solve such a problem and thus avoid to violate the Null Energy Condition (NEC).

Concerning the comparison with ΛCDM scenario, for the combined data set analysis we find that ΔAICc implies that ΛCDM is strongly favoured over Kaniadakis-holographic dark energy. This result is also supported by BIC, for which ΔBIC gives a strong evidence against it. Notice that these comparisons were performed by using the same data sets for both models ΛCDM and Kaniadakis cosmology.

Finally, based on the combined (CC + SNIa + BAO) analysis, in Fig. 2 we present the reconstruction of the Hubble parameter $H(z)$, the deceleration parameter $q(z)$ (equation (25)), and the cosmographic jerk parameter $j(z)$ (equation (26)), in the redshift range $0 < z < 2$. For comparison, we also depict the corresponding curves for ΛCDM scenario. Concerning the current values, our analysis leads to $H_0 = 76.09^{+1.06}_{-1.02}\,\mathrm{km\,s^{-1}\,Mpc^{-1}}$, $q_0 = -0.537^{+0.064}_{-0.064}$, $j_0 = 0.815^{+0.315}_{-0.274}$, where the uncertainties correspond to 1σ CL. Additionally, using the joint analysis, we find the redshift for the deceleration-acceleration transition as $z_T = 0.860^{+0.213}_{-0.138}$, and the Universe age as $t_U = 13.000^{+0.406}_{-0.350}$ Gyrs. Notice that z_T value is in agreement within 1σ with the value reported in Herrera-Zamorano, Hernández-Almada & García-Aspeitia (2020) for ΛCDM paradigm ($z_T = 0.642^{+0.014}_{-0.014}$).

4 DYNAMICAL SYSTEM AND STABILITY ANALYSIS

In this section we apply the powerful method of phase-space and stability analysis, which allows us to obtain a qualitative description of the local and global dynamics of cosmological scenarios, independently of the initial conditions and the specific evolution of the universe. The extraction of asymptotic solutions give theoretical values that can be compared with the observed ones, such as the dark-energy and total equation-of-state parameters, the deceleration parameter, the density parameters of the different sectors, etc., as well as allows the classification of the cosmological solutions (Wainwright & Ellis 1997).

In order to perform the stability analysis of a given cosmological scenario, one transforms it to its autonomous form $\mathbf{X}' = \mathbf{f(X)}$ (Ferreira & Joyce 1997; Wainwright & Ellis 1997; Copeland, Liddle & Wands 1998; Perko 2000; Coley 2003; Copeland et al. 2006; Chen, Gong & Saridakis 2009; Giambo & Miritzis 2010; Cotsakis & Kittou 2013), where $\mathbf{X}$ is the column vector containing the auxiliary variables and primes denote derivative with respect to a conveniently chosen time variable. Then, one extracts the critical points $\boldsymbol{X_c}$ by imposing the condition $\boldsymbol{X}' = 0$ and, to determine their stability properties, one expands around them with $\mathbf{U}$ the column vector of the perturbations of the variables. Therefore, for each critical point, the perturbation equations are expanded to first order as $\boldsymbol{U}' = \boldsymbol{Q}\cdot\boldsymbol{U}$, with the matrix $\boldsymbol{Q}$ containing the coefficients of the perturbation equations. Finally, the eigenvalues of $\boldsymbol{Q}$ determine the type and stability of the critical point under consideration.

4.1 Local dynamical system formulation

In this section, we study the stability of system (17)–(18) with $\mathcal{X}$ defined in (19), in the phase space

$$\left\{(E, \Omega_{DE}) \in \mathbb{R}^2 : 3E^4\Omega_{DE}^2 - 4\beta^2c^2 \geq 0\right\}. \tag{43}$$

For generality, we keep the matter equation-of-state parameter w_m in the calculations, and it can be set to zero in the final result if needed. Since β and c appear quadratic in (17), (18), (19), and (43), these equations are invariant under the changes $c \mapsto -c$ and $\beta \mapsto -\beta$. Therefore, in this section, we focus on $\beta > 0$ and $c > 0$. When $\beta < 0$ we change β by $-\beta$ and c by $-c$ on the next discussion.

The equilibrium points dominated by dark energy (namely possessing $\Omega_{DE} = 1$) with finite H are:

(i) $L_1 : (E, \Omega_{DE}) = (\frac{\sqrt{2\beta c}}{\sqrt[4]{3}}, 1)$. This point always satisfies $-12c^2\beta^2 + 9E^4\Omega_{DE}^2 = 0$. The eigenvalues are $\{-3(w_m + 1), \infty\,\mathrm{sgn}((\sqrt{2} - 2c))\}$. It is a stable point for $c > \frac{\sqrt{2}}{2}$ and $w_m > -1$, and a saddle for $c < \frac{\sqrt{2}}{2}$ and $w_m > -1$.

(ii) $L_2 : (E, \Omega_{DE}) = (\frac{\sqrt{\beta}}{\sqrt[4]{3(1-c^2)}}, 1)$. This point satisfies the reality condition if $\frac{3\beta^2(1-2c^2)^2}{1-c^2} \geq 0$, namely $\beta = 0$, $c^2 > 1$, or $\beta \neq 0$, $c^2 < 1$. For $c^2 \leq \frac{1}{2}$, the eigenvalues are

$$\lambda_1, \lambda_2 = \left\{\frac{\left(4c^4 - 4c^2 - 1\right)|c| + \left(-8c^4 + 6c^2 + 1\right)\sqrt{1 - c^2}}{\left|c - 2c^3\right|},\right.$$
$$\left. 2\left(\sqrt{\frac{1}{c^2} - 1} - 1\right)\left(2c^2 - 1\right) - 3(w_m + 1)\right\}.$$

This is a saddle point, as it can be verified numerically in Fig. 3. Moreover, for $\frac{1}{2} < c^2 < 1$, the eigenvalues are $\{2 - 2c^2, -3(w_m + 1)\}$, and thus for $w_m > -1$, it is also a saddle point.

Since $\Omega_{DE}^2 \geq \frac{4\beta^2c^2}{3E^4} \geq 0$, we deduce that the only possibility to have matter domination, namely $\Omega_{DE} = 0$, is when $E \to \infty$, due to the reality condition $c^2\beta^2 \geq 0$. It is convenient to define the dimensionless compact variable $T = (1 + E)^{-1}$ such that $T \to 0$ as $E \to \infty$ and $T \to 1$ as $E \to 0$. Then, we obtain

$$T' = \frac{3}{2}(T - 1)T(w_m + 1)(\Omega_{DE} - 1) - \frac{T^3\sqrt{\frac{(T-1)^4\Omega_{DE}^2}{T^4} - \frac{4\beta^2c^2}{3}}}{T - 1}$$
$$- \frac{T^5\sqrt{\frac{2\beta^2(T-1)^4\Omega_{DE}^2}{T^4} - \frac{8\beta^4c^2}{3}}}{(T - 1)^2\sqrt{3(T - 1)^2\Omega_{DE} - \sqrt{9(T - 1)^4\Omega_{DE}^2 - 12\beta^2c^2T^4}}}, \tag{44}$$

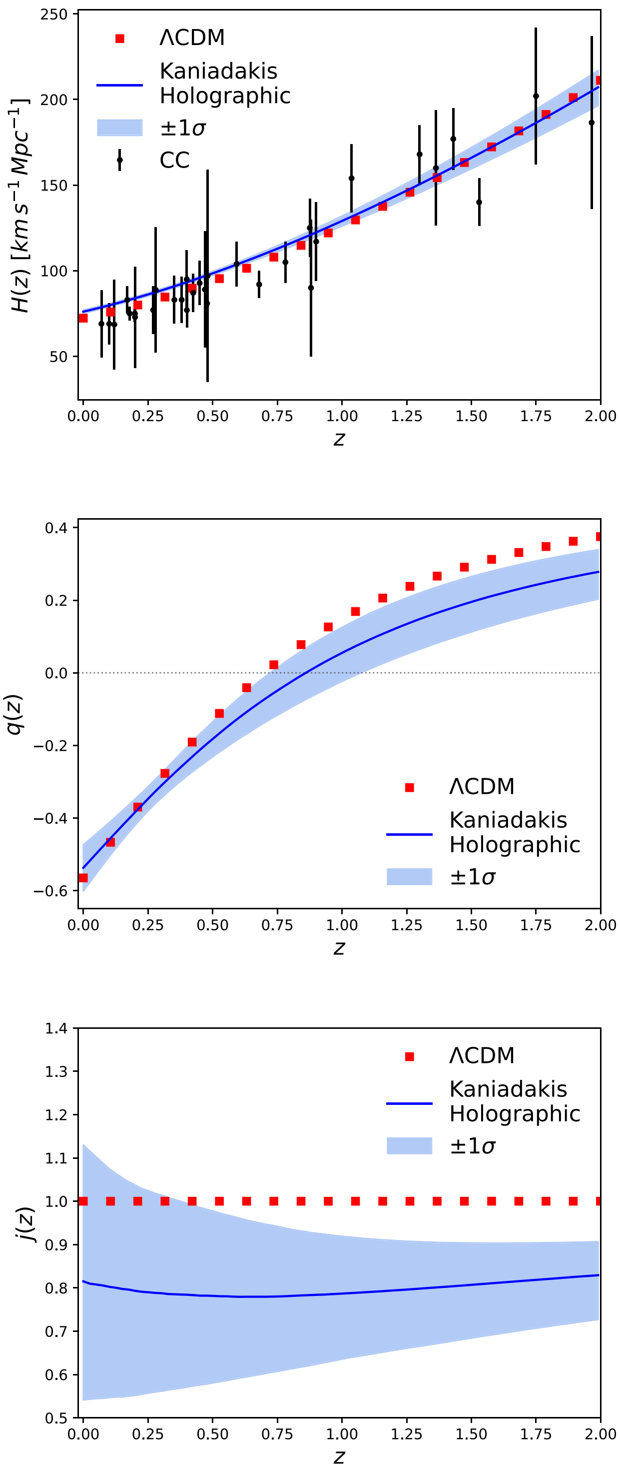

Figure 2. Reconstruction of the Hubble function ($H(z)$, upper panel), the deceleration parameter ($q(z)$, middle panel), and the jerk parameter ($j(z)$, bottom panel) for the Kanadiakis-holographic dark energy using the combined (CC + SNIa + BAO) analysis in the redshift range $0 < z < 2$. The shaded regions represent the 68 per cent CL, and the square points depict the results of the ΛCDM scenario with $h = 0.723$ and $\Omega_m^{(0)} = 0.290$, namely the values obtained through observational confrontation using the same data sets with the analysis of Kaniadakis-holographic dark energy.

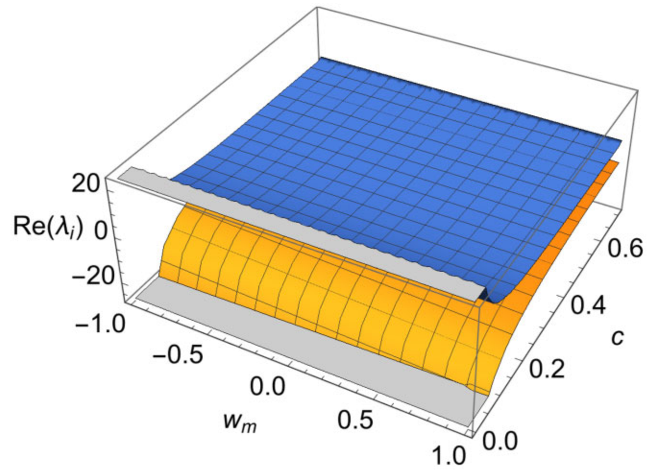

Figure 3. The eigenvalues corresponding to the point L_2, for $w_m \in [-1, 1]$, $c \in [0, \sqrt{2}/2]$.

$$\Omega'_{DE} = (\Omega_{DE} - 1)\left[-3(w_m+1)\Omega_{DE} + \frac{2T^2\sqrt{\frac{(T-1)^4\Omega_{DE}^2}{T^4} - \frac{4\beta^2c^2}{3}}}{(T-1)^2} + \frac{2T^2\sqrt{2\beta^2(T-1)^4\Omega_{DE}^2 - \frac{8}{3}\beta^4c^2T^4}}{(T-1)^3\sqrt{3(T-1)^2\Omega_{DE} - \sqrt{9(T-1)^4\Omega_{DE}^2 - 12\beta^2c^2T^4}}}\right], \quad (45)$$

defined on the physical region

$$9(T-1)^4\Omega_{DE}^2 - 12\beta^2c^2T^4 \geq 0. \quad (46)$$

In summary, the sources/sinks are:

(i) $L_1 : (E, \Omega_{DE}) = (\frac{\sqrt{2\beta c}}{\sqrt[4]{3}}, 1)$ is a stable point for $c > \frac{\sqrt{2}}{2}$ and $w_m > -1$, and a saddle for $c < \frac{\sqrt{2}}{2}$ and $w_m > -1$.

(ii) For a dark-energy-dominated solution L_3: $(T, \Omega_{DE}) = (0, 1)$, the eigenvalues are $\{\frac{c-1}{c}, -\frac{3cw_m+c+2}{c}\}$, thus it is a stable point for $-1 < w_m < 1$ and $0 < c < 1$ or a saddle for $-1 < w_m < 1$ and $c > 1$.

(iii) The past attractor is the matter-dominated solution L_4: $(T, \Omega_{DE}) = (0, 0)$, for which the eigenvalues are $\{3(w_m+1), \frac{3(w_m+1)}{2}\}$, and since they are always positive for $-1 < w_m < 1$, it is an unstable point.

We remark here that $E = E_c$ finite corresponds to the de Sitter solution with $H = E_c H_0$, and $a(t) \propto e^{E_c H_0 t}$. That is, point L_1 satisfies $a(t) \propto e^{\frac{\sqrt{2|\beta c|}}{\sqrt[4]{3}} H_0 t}$ and it is a late-time attractor providing the accelerated regime. Additionally, for $\beta \neq 0$, $c^2 < 1$, the point L_2 exists and satisfies $a(t) \propto e^{\frac{\sqrt{|\beta|}}{\sqrt[4]{3(1-c^2)}} H_0 t}$, and since it is a saddle it can provide a transient accelerated phase that can be related to inflation.

In order to present the results in a more transparent way, in Fig. 4, we show a phase-space plot of the system (44)–(45) for the best-fitting values $\beta = -0.003$ and $c = 1.151$ and for dust matter ($w_m = 0$). The red curve represents the solution for the initial data $\Omega_{DE}|_{z=0} = 0.71$, corresponding to the mean value from the joint analysis CC+SNIa + BAO, and for $T|_{z=0} = 0.5$. The dashed blue region is the physical region $9(T-1)^4\Omega_{DE}^2 - 12\beta^2c^2T^4 \geq 0$, where the equations are real-valued. From this figure, it is confirmed that the late-time attractor is a dark-energy-dominated solution $\Omega_{DE} = 1$ with $T = 0$. The past attractor is the matter-dominated solution $\Omega_{DE} = 0$ with $T = 0$. At the finite region, point L_1 is the stable one.

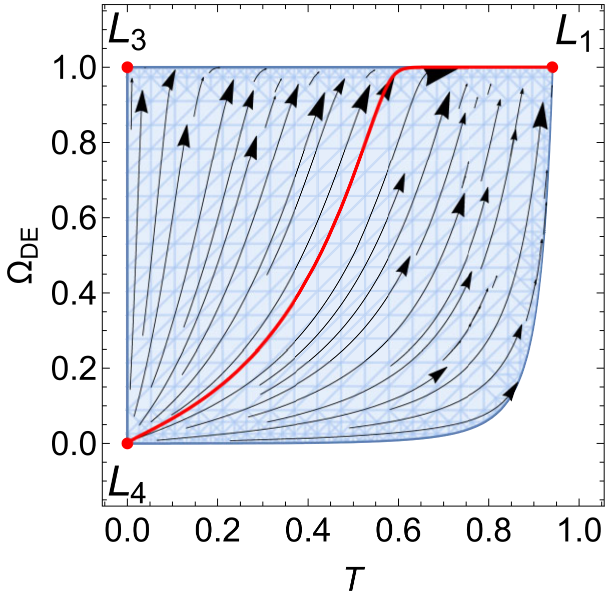

Figure 4. Phase-space plot of the dynamical system (44)–(45), for the best-fitting values $\beta = -0.003$ and $c = 1.151$ of Kaniadakis-holographic dark energy, and for dust matter ($w_m = 0$). The red curve represents the solution for the initial data $\Omega_{DE}|_{z=0} = 0.71$, corresponding to the mean value from the joint analysis CC + SNIa + BAO, and for $T|_{z=0} = 0.5$. The dashed blue region is the physical region $9(T-1)^4\Omega_{DE}^2 - 12\beta^2c^2T^4 \geq 0$, where the equations are real-valued.

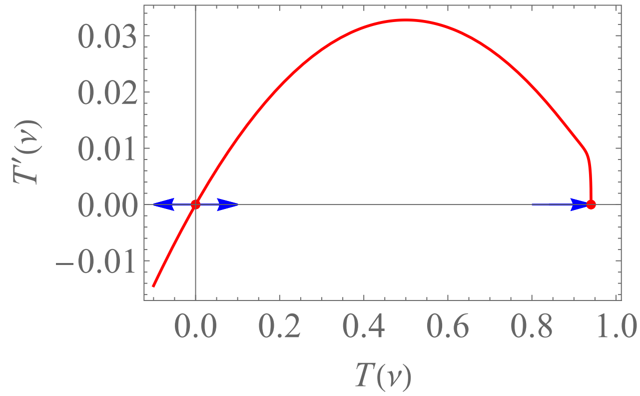

Figure 5. Phase-space plot of the 1D dynamical system (47), for the best-fitting values $\beta = -0.003$ and $c = 1.151$ of Kaniadakis-holographic dark energy. The equilibrium point $T = 0$ is unstable, while the de Sitter equilibrium point $T = T_c \approx 0.941$ is stable.

Setting $\Omega_{DE} = 1$, the system (44)–(45) becomes a 1D dynamical system:

$$T' = \frac{T^3\sqrt{\frac{(T-1)^4}{T^4} - \frac{4\beta^2c^2}{3}}}{1-T} - \frac{T^3\sqrt{2\beta^2(T-1)^4 - \frac{8}{3}\beta^4c^2T^4}}{(T-1)^2\sqrt{3(T-1)^2 - \sqrt{9(T-1)^4 - 12\beta^2c^2T^4}}}. \quad (47)$$

The origin $T = 0$ has eigenvalue $\lambda = 1 - \frac{1}{|c|}$. Moreover, the system admits, at most, four additional equilibrium points T_c, with $T_c \in \{T_1, T_2, T_3, T_4\}$ satisfying $\frac{(T-1)^4}{T^4} - \frac{4\beta^2c^2}{3} = 0$. Explicitly, we have that

$$T_{1,2} = \frac{3}{3-4\beta^2c^2} - \frac{2\sqrt{3}|c\beta|}{|3-4c^2\beta^2|} \mp \frac{\sqrt{2}\sqrt{12|c\beta|\,|3-4c^2\beta^2| + \sqrt{3}\left(16\beta^4c^4 - 9\right)}\sqrt{|c\beta|}}{|3-4c^2\beta^2|^{3/2}}, \quad (48a)$$

$$T_{3,4} = \frac{3}{3-4\beta^2c^2} + \frac{2\sqrt{3}|c\beta|}{|3-4c^2\beta^2|} \mp \frac{\sqrt{2}\sqrt{12|c\beta|\,|3-4c^2\beta^2| + \sqrt{3}\left(9 - 16\beta^4c^4\right)}\sqrt{|c\beta|}}{|3-4c^2\beta^2|^{3/2}}. \quad (48b)$$

Such points with $0 < T_c < 1$, corresponding to de Sitter solution $a(t) \propto e^{H_0t(\frac{1}{T_c}-1)}$, are stable for $c \geq 1$ and otherwise are saddle.

For the best-fitting values $\beta = -0.003$ and $c = 1.151$, the origin has eigenvalue $\lambda \approx 0.13$, and therefore it is a source. In this case the only real value is $T_3 \approx 0.941$. The exact eigenvalue is negative infinity (for $c \geq 1$) at the exact value of T_3, and therefore it is stable. In Fig. 5, we draw a phase-space plot of the 1D dynamical system (47), for the best-fitting values $\beta = -0.003$ and $c = 1.151$ of Kaniadakis-holographic dark energy. The equilibrium point $T = 0$ is unstable, while the de Sitter equilibrium point $T = T_c \approx 0.941$ is stable.

4.2 Global dynamical systems formulation

In the previous section, we performed the local analysis of the scenario. However, due to the presence of rational functions that are not analytic in the whole domain, it becomes necessary to investigate the full global dynamics. We start by defining the dimensionless variables θ, T as

$$T = \frac{H_0}{H + H_0} = \frac{1}{1+E}, \quad \theta = \arcsin\left(\sqrt{1 - \frac{\rho_{DE}}{3M_p^2H^2}}\right), \quad (49)$$

such that

$$\sin^2(\theta) = \frac{\rho_m}{3M_p^2H^2}, \quad \cos^2(\theta) = \frac{\rho_{DE}}{3M_p^2H^2}. \quad (50)$$

For an expanding universe ($H > 0$), we have that $T \in [0, 1]$, while θ is a periodic coordinate and, thus, we can set $\theta \in [-\pi, \pi]$. Therefore, we obtain a global phase-space formulation.

4.2.1 *Standard holographic dark energy ($\beta = 0$)*

In order to present the features of Kaniadakis-holographic dark energy in comparison with standard-holographic dark energy, we first analyse the latter case for completeness, namely we consider the system (28)–(29) for $\beta = 0$. In this case, we obtain

$$T' = \frac{(T-1)T\left\{\cos^2(\theta)[(3w_m+1)c + 2\cos(\theta)] - 3c(w_m+1)\right\}}{2c}, \quad (51)$$

$$\theta' = -\frac{[(3w_m+1)c + 2\cos(\theta)]\sin(2\theta)}{4c}. \quad (52)$$

The critical points of the above system, alongside their associated eigenvalues, are presented in Table 2. Note that θ is unique modulo 2π, and focus on $\cos\theta \geq 0$. In the following list, $\arctan[x, y]$ gives the arc tangent of y/x, taking into account on which quadrant the point (x, y) is in. When $x^2 + y^2 = 1$, $\arctan[x, y]$ gives the number θ such that $x = \cos\theta$ and $y = \sin\theta$.

Table 2. The critical points and their associated eigenvalues of the system (51)–(52) for $\beta = 0$ in (28)–(29), namely for the case of standard holographic dark energy. We use the notation $x = \frac{1}{2}c(3w_m + 1)$, while $c_1 \in \mathbb{Z}$.

Label	(T, θ)	Eigenvalues
P_1	$(0, 2\pi c_1)$	$\left\{\frac{c-1}{c}, -\frac{3w_m c+c+2}{2c}\right\}$
P_2	$\left(0, \frac{1}{2}\pi\,(4c_1 - 1)\right)$	$\left\{\frac{3(w_m+1)}{2}, \frac{1}{2}(3w_m + 1)\right\}$
P_3	$\left(0, \frac{1}{2}\pi\,(4c_1 + 1)\right)$	$\left\{\frac{3(w_m+1)}{2}, \frac{1}{2}(3w_m + 1)\right\}$
$P_4^{\pm}$	$(0, 2\pi c_1 \pm \pi)$	$\left\{1 + \frac{1}{c}, -\frac{3w_m}{2} + \frac{1}{c} - \frac{1}{2}\right\}$
P_5	$\left(0, \arctan\left[-x, -\sqrt{1-x^2}\right] + 2\pi c_1\right)$	$\left\{\frac{3(w_m+1)}{2}, \frac{1}{8}(3w_m + 1)\left(c^2(1 + 3w_m)^2 - 4\right)\right\}$
P_6	$\left(0, \arctan\left[-x, \sqrt{1-x^2}\right] + 2\pi c_1\right)$	$\left\{\frac{3(w_m+1)}{2}, \frac{1}{8}(3w_m + 1)\left(c^2(1 + 3w_m)^2 - 4\right)\right\}$
P_7	$(1, 2\pi c_1)$	$\left\{\frac{1}{c} - 1, -\frac{3w_m c+c+2}{2c}\right\}$
P_8	$\left(1, \frac{1}{2}\pi\,(4c_1 - 1)\right)$	$\left\{-\frac{3}{2}(w_m + 1), \frac{1}{2}(3w_m + 1)\right\}$
P_9	$\left(1, \frac{1}{2}\pi\,(4c_1 + 1)\right)$	$\left\{-\frac{3}{2}(w_m + 1), \frac{1}{2}(3w_m + 1)\right\}$
$P_{10}^{\pm}$	$(1, 2\pi c_1 \pm \pi)$	$\left\{-\frac{c+1}{c}, -\frac{3w_m}{2} + \frac{1}{c} - \frac{1}{2}\right\}$
P_{11}	$\left(1, \arctan\left[-x, -\sqrt{1-x^2}\right] + 2\pi c_1\right)$	$\left\{-\frac{3}{2}(w_m + 1), \frac{1}{8}(3w_m + 1)\left(c^2(1 + 3w_m)^2 - 4\right)\right\}$
P_{12}	$\left(1, \arctan\left[-x, \sqrt{1-x^2}\right] + 2\pi c_1\right)$	$\left\{-\frac{3}{2}(w_m + 1), \frac{1}{8}(3w_m + 1)\left(c^2(1 + 3w_m)^2 - 4\right)\right\}$

In summary, in the case $\beta = 0$, the critical points can be completely characterized. In particular:

(i) Point P_1 always exists. It corresponds to a dark-energy-dominated solution, i.e. $\Omega_{DE} = 1$ with $T = 0$. It is a stable point for $-1 < w_m < 1$, $0 < c < 1$.

(ii) Points P_2 and P_3 exist always. They are two representations of the matter-dominated solution $\Omega_{DE} = 0$ with $T = 0$. They are past attractors, i.e. unstable points, for $-\frac{1}{3} < w_m \leq 1$, while they are saddle for $-1 < w_m < -\frac{1}{3}$.

(iii) Points $P_4^{\pm}$ exist always. They correspond to a dark-energy-dominated solution with $\Omega_{DE} = 1$ with $T = 0$. They are unstable points for $0 < c < \frac{1}{2}, -1 \leq w_m \leq 1$, or $c \geq \frac{1}{2}$, $\quad -1 \leq w_m < \frac{2-c}{3c}$, while they are saddle for $c > \frac{1}{2}$, $\quad \frac{2-c}{3c} < w_m \leq 1$.

(iv) Points P_5 and P_6 exist for $-1 \leq \frac{1}{2}c(3w_m + 1) \leq 1$. They are sources for $0 \leq c \leq 1$, $\quad -1 < w_m < -\frac{1}{3}$ or $c > 1$, $\quad -\frac{c+2}{3c} < w_m < -\frac{1}{3}$. For $0 \leq c < \frac{1}{2}$, $\quad -\frac{1}{3} < w_m \leq 1$, or $c \geq \frac{1}{2}$, $\quad -\frac{1}{3} < w_m < \frac{2-c}{3c}$, they are saddle.

(v) Point P_7 exists always. It corresponds to a dark-energy-dominated solution $\Omega_{DE} = 1$ with $T = 1$. It is a stable point for $c > 1$, $\quad -\frac{c+2}{3c} < w_m \leq 1$.

(vi) Points P_8 and P_9 exist always. They are two representations of the matter-dominated solution $\Omega_{DE} = 0$ with $T = 1$. They are stable points for $-1 < w_m < -\frac{1}{3}$, while they are saddle points for $-\frac{1}{3} < w_m \leq 1$.

(vii) Points $P_{10}^{\pm}$ are two representations of the matter-dominated solution $\Omega_{DE} = 0$ with $T = 1$. They are stable points for $c > \frac{1}{2}$, $\frac{2-c}{3c} < w_m \leq 1$, while they are saddle for $0 < c < \frac{1}{2}$, $\quad -1 \leq w_m \leq 1$, or $c \geq \frac{1}{2}$, $\quad -1 \leq w_m < \frac{2-c}{3c}$.

(viii) Points P_{11} and P_{12} exist for $-1 \leq \frac{1}{2}c(3w_m + 1) \leq 1$. They are saddle for $0 \leq c \leq 1$, $\quad -1 < w_m < -\frac{1}{3}$, or $c > 1$, $\quad -\frac{c+2}{3c} < w_m < -\frac{1}{3}$, while for $0 \leq c < \frac{1}{2}$, $\quad -\frac{1}{3} < w_m \leq 1$, or $c \geq \frac{1}{2}$, $\quad -\frac{1}{3} < w_m < \frac{2-c}{3c}$, they are stable.

In order to give a better picture of the system behaviour, Fig. 6 displays a phase-space plot of the system (51)–(52) for $\beta = 0$ in (28)–(29), and dust matter. The red curve corresponds to the universe evolution according to parameter mean values from the joint analysis. From this figure, we deduce that the late-time attractor is a dark-energy-dominated solution with $\Omega_{DE} = 1$ and $T = 1$ (point P_7),

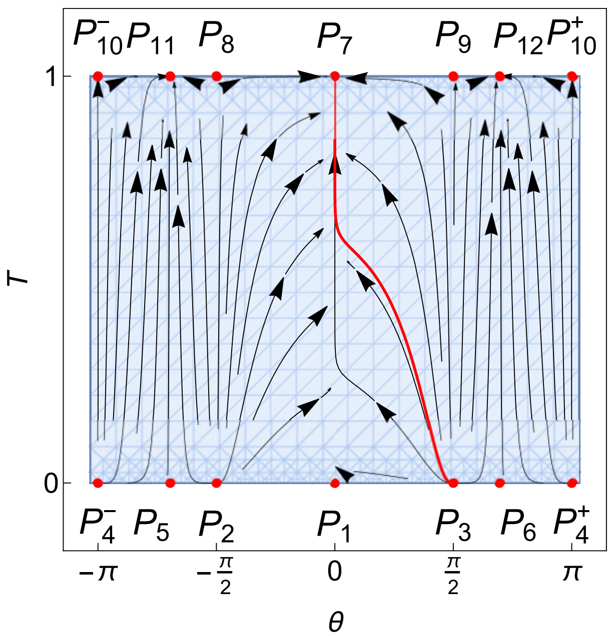

Figure 6. Phase-space plot of the dynamical system (51)–(52) for $\beta = 0$ in (28)–(29), namely for standard holographic dark energy, for the value $c = 1.151$, and for dust matter $w_m = 0$. The red curve represents the solution for the initial data $\Omega_{DE}|_{z=0} = 0.71$ (i.e. $\theta(0) = \arccos(\frac{1}{10}\sqrt{71}) \approx 0.569$), corresponding to the mean value obtained with the joint analysis CC + SNIa + BAO, and for $T|_{z=0} = 0.5$. The dashed blue region is the physical region where the equations are real-valued.

while the past attractor is the matter-dominated solution with $\Omega_{DE} = 0$ and $T = 0$ (point P_3). For other initial conditions there are other late-time attractors, such as points P_{11} and P_{12} which are stable for the best-fitting parameters since they satisfy $c \geq \frac{1}{2}$, $\quad -\frac{1}{3} < w_m < \frac{2-c}{3c}$. These points are scaling solutions since they have $\Omega_{DE} = x^2$ and $\Omega_{DM} = 1 - x^2$, with $x = \frac{c}{2}(3w_m + 1) = \frac{c}{2}$ for $w_m = 0$. Additionally, points P_2, P_3, which are matter-dominated solutions, and points $P_4^{\pm}$, which are dark-energy-dominated solutions, are also past attractors.

Table 3. The critical points and their associated eigenvalues of the system (53)–(54) in the invariant set $T = 0$. We use the notation $x = \frac{1}{2}c(3w_m + 1)$, $c_1 \in \mathbb{Z}$.

Label	(T, θ)	Eigenvalues
P_1	$(0, 2\pi c_1)$	$\left\{\frac{c-1}{c}, -\frac{3w_m c+c+2}{2c}\right\}$
P_2	$\left(0, \frac{1}{2}\pi\,(4c_1 - 1)\right)$	$\left\{\frac{3(w_m+1)}{2}, \frac{1}{2}(3w_m + 1)\right\}$
P_3	$\left(0, \frac{1}{2}\pi\,(4c_1 + 1)\right)$	$\left\{\frac{3(w_m+1)}{2}, \frac{1}{2}(3w_m + 1)\right\}$
$P_4^{\pm}$	$(0, 2\pi c_1 \pm \pi)$	$\left\{1 + \frac{1}{c}, -\frac{3w_m}{2} + \frac{1}{c} - \frac{1}{2}\right\}$
P_5	$\left(0, \arctan\left[-x, -\sqrt{1-x^2}\right] + 2\pi c_1\right)$	$\left\{\frac{3(w_m+1)}{2}, \frac{1}{8}(3w_m + 1)\left(c^2(1 + 3w_m)^2 - 4\right)\right\}$
P_6	$\left(0, \arctan\left[-x, \sqrt{1-x^2}\right] + 2\pi c_1\right)$	$\left\{\frac{3(w_m+1)}{2}, \frac{1}{8}(3w_m + 1)\left(c^2(1 + 3w_m)^2 - 4\right)\right\}$

4.2.2 Kaniadakis-holographic dark energy ($\beta \neq 0$)

Let us now investigate the full extended model of Kaniadakis-holographic dark energy, namely the general case where $\beta \neq 0$. The full system (17)–(18) becomes

$$T' = \frac{3}{2}(1-T)T(w_m+1)\sin^2(\theta) + \frac{T^3\sqrt{\frac{(1-T)^4\cos^4(\theta)}{T^4} - \frac{4\beta^2c^2}{3}}}{1-T} - \frac{T^5\sqrt{\frac{18(1-T)^4\cos^4(\theta)\beta^2}{T^4} - 24\beta^4c^2}}{3(T-1)^2\sqrt{3(T-1)^2\cos^2(\theta) - \sqrt{9(1-T)^4\cos^4(\theta) - 12\beta^2c^2T^4}}}, \quad (53)$$

$$\theta' = -\frac{3}{4}(w_m+1)\sin(2\theta) + \frac{T^2\tan(\theta)\sqrt{\frac{(1-T)^4\cos^4(\theta)}{T^4} - \frac{4\beta^2c^2}{3}}}{(T-1)^2} - \frac{\sqrt{\frac{2}{3}}T^2\tan(\theta)\sqrt{-\beta^2\left(4\beta^2c^2T^4 - 3(1-T)^4\cos^4(\theta)\right)}}{(1-T)^3\sqrt{3(T-1)^2\cos^2(\theta) - \sqrt{9(1-T)^4\cos^4(\theta) - 12\beta^2c^2T^4}}}. \quad (54)$$

Moreover, the physical region of the phase space is

$$3(1-T)^4\cos^4(\theta) - 4\beta^2c^2T^4 \geq 0. \quad (55)$$

We proceed by studying the critical points of the system (53)–(54) in the physical region (55) and their stability. We mention that for $\beta \neq 0$ the invariant set $T = 1$ is not physical. Near the invariant set $T = 0$, the system (53)–(54) becomes

$$T' = \left[-\frac{\cos^3(\theta)}{c} + \cos^2(\theta) + \frac{3}{2}(w_m+1)\sin^2(\theta)\right]T + O\left(T^2\right), \quad (56)$$

$$\theta' = -\frac{[(3w_m+1)c + 2\cos(\theta)]\sin(2\theta)}{4c} + O\left(T^2\right). \quad (57)$$

In Table 3, we summarize the critical points P_1 to P_6, alongside their associated eigenvalues. Furthermore, the stability conditions are the same as discussed in Section 4.2.1. In summary, in the invariant set $T = 0$, the critical points are:

(i) Point P_1 exists always. It corresponds to a dark-energy-dominated solution, i.e. $\Omega_{DE} = 1$ with $T = 0$. It is a stable point for $-1 < w_m < 1$, $0 < c < 1$.

(ii) Points P_2 and P_3 exist always. They are two representations of the matter-dominated solution $\Omega_{DE} = 0$ with $T = 0$. They are past attractors, i.e. unstable points, for $-\frac{1}{3} < w_m \leq 1$, while they are saddle for $-1 < w_m < -\frac{1}{3}$.

(iii) Point $P_4^{\pm}$ exist always. They correspond to a dark-energy-dominated solution with $\Omega_{DE} = 1$ with $T = 0$. They are unstable points for $0 < c < \frac{1}{2}$, $-1 \leq w_m \leq 1$, or $c \geq \frac{1}{2}$, $-1 \leq w_m < \frac{2-c}{3c}$, while they are saddle for $c > \frac{1}{2}$, $\frac{2-c}{3c} < w_m \leq 1$.

(iv) Points P_5 and P_6 exist for $-1 \leq \frac{1}{2}c(3w_m + 1) \leq 1$. They are unstable for $0 \leq c \leq 1$, $-1 < w_m < -\frac{1}{3}$, or $c > 1$, $-\frac{c+2}{3c} < w_m < -\frac{1}{3}$, while for $0 \leq c < \frac{1}{2}$, $-\frac{1}{3} < w_m \leq 1$, or $c \geq \frac{1}{2}$, $-\frac{1}{3} < w_m < \frac{2-c}{3c}$, they are saddle.

Moreover, the system admits, at most, 12 additional equilibrium points (θ, T), with $\theta \in \{\theta_1, \theta_2, \theta_3\}$ satisfying $\cos^2(\theta) = 1$, and $T \in \{T_1, T_2, T_3, T_4\}$ satisfying $\frac{(T-1)^4}{T^4} - \frac{4\beta^2c^2}{3} = 0$, explicitly given by (48). Such points with $0 < T_c < 1$, corresponding to de Sitter solution $a(t) \propto e^{H_0 t\left(\frac{1}{T_c}-1\right)}$, are stable for $c \geq 1$ or saddle otherwise.

Notice that the physical values are the real values of T_i satisfying $0 \leq T_i \leq 1$, $i = 1, 2, 3, 4$. One eigenvalue is always $-\frac{3}{2}(1 + w_m)$, while the other one is infinite. The stability conditions are found numerically and, moreover, for $\beta = 0$, we find $T_i = 0$. Hence, we re-obtain points P_7 and $P_{10}^{\pm}$ in Table 2. Indeed, for $\beta = 0$, all the results of Section 4.2.1 are recovered.

The solutions of physical interest are those with $T = 0$. Point P_1, which corresponds to a dark-energy-dominated solution $\Omega_{DE} = 1$ with $T = 0$, is stable for $-1 < w_m < 1$, $0 < c < 1$. Points P_2 and P_3, which are two representations of the matter-dominated solution $\Omega_{DE} = 0$ with $T = 0$, are past attractors for $-\frac{1}{3} < w_m \leq 1$ or saddle for $-1 < w_m < -\frac{1}{3}$. Point $P_4^{\pm}$, which corresponds to a dark-energy-dominated solution are unstable for $0 < c < \frac{1}{2}$, $-1 \leq w_m \leq 1$, or $c \geq \frac{1}{2}$, $-1 \leq w_m < \frac{2-c}{3c}$, while they are saddle points for $c > \frac{1}{2}$, $\frac{2-c}{3c} < w_m \leq 1$. Finally, points P_5 and P_6 exist for $-1 \leq \frac{1}{2}c(3w_m + 1) \leq 1$. They are sources for $0 \leq c \leq 1$, $-1 < w_m < -\frac{1}{3}$ or $c > 1$, $-\frac{c+2}{3c} < w_m < -\frac{1}{3}$, while for $0 \leq c < \frac{1}{2}$, $-\frac{1}{3} < w_m \leq 1$, or $c \geq \frac{1}{2}$, $-\frac{1}{3} < w_m < \frac{2-c}{3c}$, they are saddle. Finally, note that the region where $T \to 1$ is contained in the complex-valued domain. This forbids solutions with $H = 0$, which appear in the standard-holographic dark energy scenario of (51)–(52).

In Fig. 7 we show a phase-space plot of the system (53)–(54) for the best-fitting values $\beta = -0.003$ and $c = 1.151$ and for dust matter ($w_m = 0$). In this case, the only real value is $T_3 \approx 0.941$. At points $(-\pi, T_3)$, $(0, T_3)$, and (π, T_3), the eigenvalues are $-\frac{3}{2}$ and one eigenvalue is negative infinity at the exact value of T_3, therefore they are sink. For comparison, we have added the red curve, corresponding to the solution for the initial data $\Omega_{DE}|_{z=0} = 0.71$ (i.e. $\theta(0) = \arccos(\frac{1}{10}\sqrt{71}) \approx 0.569$), which is the mean value from the joint analysis CC + SNIa + BAO, and for $T|_{z=0} = 0.5$. From this figure, it is confirmed that the late-time attractor is a dark-energy dominated solution (de Sitter solution with $a(t) \propto e^{H_0 t\left(\frac{1}{T_c}-1\right)}$, $H_0 = h \times 100\,\mathrm{km\,s^{-1}Mpc^{-1}}$, $T_c \approx 0.941$, $h = 0.761$), while the past attractor is the matter-dominated solution.

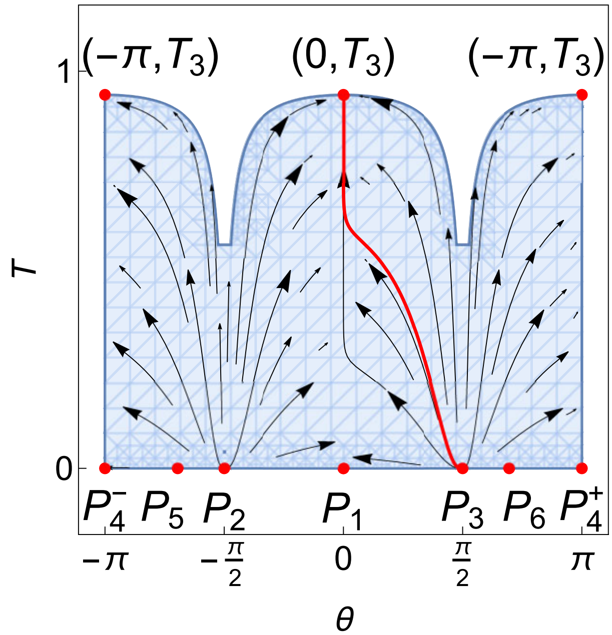

Figure 7. Phase-space plot of the dynamical system (53)–(54) for the best-fitting values $\beta = -0.003$ and $c = 1.151$, and for dust matter ($w_m = 0$). The red curve represents the solution for the initial data $\Omega_{DE}|_{z=0} = 0.71$ (i.e. $\theta(0) = \arccos(\frac{1}{10}\sqrt{71}) \approx 0.569$), corresponding to the mean value from the joint analysis CC + SNIa + BAO, and for $T|_{z=0} = 0.5$. The dashed blue region is the physical region where the equations are real-valued.

5 SUMMARY AND DISCUSSION

We investigated the scenario of Kaniadakis-holographic dark energy scenario by confronting it with observational data. This is an extension of the usual holographic dark-energy model that arises from the use of the generalized Kaniadakis entropy instead of the standard Boltzmann-Gibbs one, which in turn appear from the relativistic extension of a standard statistical theory.

We applied the Bayesian approach to extract the likelihood bounds of the Kaniadakis parameter, as well as the other free model parameters. In particular, we performed a MCMC analysis using data from cosmic chronometers, SNIa type Ia, and BAOs observations. Concerning the Kaniadakis parameter, we found that it is constrained around 0, namely, around the value in which Kaniadakis entropy recovers the standard Bekenstein-Hawking one, as expected. Additionally, for $\Omega_m^{(0)}$, we obtained a slightly smaller value compared to ΛCDM scenario.

Furthermore, we reconstructed the evolution of the Hubble, deceleration, and jerk parameters in the redshift range $0 < z < 2$. We find that, within one sigma CL with those reported in Herrera-Zamorano et al. (2020), the deceleration-acceleration transition redshift is $z_T = 0.86^{+0.21}_{-0.14}$, and the age of the Universe is $t_U = 13.000^{+0.406}_{-0.350}$ Gyrs. Lastly, we applied the usual information criteria in order to compare the statistical significance of the fittings with ΛCDM cosmology. Both criteria AICc and BIC conclude that the ΛCDM scenario is strongly favoured in comparison to Kaniadakis-holographic dark energy.

Finally, we performed a detailed dynamical-system analysis to extract the local and global features of the evolution in the scenario of Kaniadakis-holographic dark energy. We extracted the critical points, as well as their stability properties, and found that the past attractor of the Universe is the matter-dominated solution, while the late-time stable solution is the dark-energy-dominated one with $H \to 0$.

In summary, Kaniadakis-holographic dark energy presents interesting cosmological behaviour and is in agreement with observations. We remark that the scenario may solve the turning point in the Hubble parameter reconstruction of standard holographic dark energy (Colgáin & Sheikh-Jabbari 2021), which violates the NEC, and thus it is an interesting improvement in this context.

ACKNOWLEDGEMENTS

We thank the anonymous referee for thoughtful remarks and suggestions. Authors acknowledge Eoin O. Colgain for fruitful comments. GL was funded by Agencia Nacional de Investigación y Desarrollo - ANID for financial support through the program FONDECYT Iniciación grant no. 11180126 and by Vicerrectoría de Investigación y Desarrollo Tecnológico at UCN. JM acknowledges the support from ANID project Basal AFB-170002 and ANID REDES 190147. MAG-A acknowledges support from SNI-México, CONACyT research fellow, ANID REDES (190147), Cátedra Marcos Moshinsky, and Instituto Avanzado de Cosmología (IAC). AHA thanks to the PRODEP project, Mexico for resources and financial support and thanks also to the support from Luis Aguilar, Alejandro de León, Carlos Flores, and Jair García of the Laboratorio Nacional de Visualización Científica Avanzada. VM acknowledges support from Centro de Astrofísica de Valparaíso and ANID REDES 190147. This work is partially supported by the Ministry of Education and Science of the Republic of Kazakhstan, grant AP08856912.

DATA AVAILABILITY

The data underlying this article were cited in Section 3.1.

REFERENCES

Abreu E. M. C., Ananias Neto J., 2021, Europhys. Lett., 133, 49001
Abreu E. M. C., Ananias Neto J., Barboza E. M., Nunes R. C., 2016, Europhys. Lett., 114, 55001
Abreu E. M. C., Neto J. A., Mendes A. C. R., Bonilla A., 2018, Europhys. Lett., 121, 45002
Aghanim N. et al., 2020, A&A, 641, A6
Akaike H., 1974, IEEE Trans. Autom. Control, 19, 716
Aylor K., Joy M., Knox L., Millea M., Raghunathan S., Wu W. L. K., 2019, ApJ, 874, 4
Bhattacharjee S., 2021, Eur. Phys. J. C, 81, 217
Birrer S., Treu T., 2021, A&A, 649, A61
Bouhmadi-Lopez M., Errahmani A., Ouali T., 2011, Phys. Rev. D, 84, 083508
Cai R.-G., 2007, Phys. Lett. B, 657, 228
Cai Y.-F., Saridakis E. N., Setare M. R., Xia J.-Q., 2010, Phys. Rep., 493, 1
Cai Y.-F., Capozziello S., De Laurentis M., Saridakis E. N., 2016, Rep. Prog. Phys., 79, 106901
Capozziello S., De Laurentis M., 2011, Phys. Rep., 509, 167
Chaplygin S. A., 1904, Sci. Mem. Moscow Univ. Math. Phys., 21
Chen X.-M., Gong Y.-g., Saridakis E. N., 2009, J. Cosmol. Astropart. Phys., 0904, 001
Coley A. A., 2003, Dynamical Systems and Cosmology, Vol. 291. Springer, Dordrecht
Colgáin E. O., Sheikh-Jabbari M. M., 2021, Class. Quantum Gravity, 38, 177001
Copeland E. J., Liddle A. R., Wands D., 1998, Phys. Rev., D57, 4686
Copeland E. J., Sami M., Tsujikawa S., 2006, Int. J. Mod. Phys. D, 15, 1753
Cotsakis S., Kittou G., 2013, Phys. Rev., D88, 083514
Cruz M., Cruz N., Lepe S., 2017a, Phys. Rev. D, 96, 124020

Cruz N., Hernández-Almada A., Cornejo-Pérez O., 2019, Phys. Rev. D, 100, 083524
da Silva W. J. C., Silva R., 2021, Eur. Phys. J. Plus, 136, 543
Dabrowski M. P., Salzano V., 2020, Phys. Rev. D, 102, 064047
Dainotti M. G., De Simone B., Schiavone T., Montani G., Rinaldi E., Lambiase G., 2021, ApJ, 912, 150
Di Valentino E. et al., 2021, Astropart. Phys., 131, 102605
Drepanou N., Lymperis A., Saridakis E. N., Yesmakhanova K., 2021, Kaniadakis-Holographic Dark Energy. preprint (arXiv:2109.09181)
Efstathiou G., 2021, MNRAS, 505, 3866
Feng C., Wang B., Gong Y., Su R.-K., 2007, J. Cosmol. Astropart. Phys., 09, 005
Ferreira P. G., Joyce M., 1997, Phys. Rev. Lett., 79, 4740
Foreman-Mackey D., Hogg D. W., Lang D., Goodman J., 2013, PASP, 125, 306
Freedman W. L., 2021, ApJ, 919, 16
García-Aspeitia M. A., Hernández-Almada A., 2021, Phys. Dark Univ., 32, 100799
García-Aspeitia M. A., Magaña J., Hernández-Almada A., Motta V., 2017, Int. J. Mod. Phys. D, 27, 1850006
Garcia-Aspeitia M. A., Hernandez-Almada A., Magaña J., Amante M. H., Motta V., Martínez-Robles C., 2018, Phys. Rev. D, 97, 101301
García-Aspeitia M. A., Martínez-Robles C., Hernández-Almada A., Magaña J., Motta V., 2019, Phys. Rev., D99, 123525
García-Aspeitia M. A., Hernández-Almada A., Magaña J., Motta V., 2021, Phys. Dark Univ., 32, 100840
Giambo R., Miritzis J., 2010, Class. Quant. Grav., 27, 095003
Glavan D., Lin C., 2020, Phys. Rev. Lett., 124, 081301
Gong Y.-g., 2004, Phys. Rev. D, 70, 064029
Hernández-Almada A., 2019, Eur. Phys. J. C, 79, 751
Hernández-Almada A., Magaña, Juan García-Aspeitia, Miguel A., Motta V., 2019, Eur. Phys. J. C, 79, 12
Hernández-Almada A., García-Aspeitia M. A., Magaña J., Motta V., 2020a, Phys. Rev. D, 101, 063516
Hernández-Almada A., Leon G., Magaña J., García-Aspeitia M. A., Motta V., 2020b, MNRAS, 497, 1590
Herrera-Zamorano L., Hernández-Almada A., García-Aspeitia M. A., 2020, Eur. Phys. J. C, 80, 637
Horvat R., 2004, Phys. Rev. D, 70, 087301
Huang Q., Huang H., Xu B., Tu F., Chen J., 2021, Eur. Phys. J. C, 81, 686
Hurvich C. M., Tsai C. L., 1989, Biometrika, 76, 297
Kaniadakis G., 2002, Phys. Rev. E, 66, 056125
Kaniadakis G., 2005, Phys. Rev. E, 72, 036108
Khurshudyan M., Sadeghi J., Myrzakulov R., Pasqua A., Farahani H., 2014, Adv. High Energy Phys., 2014, 878092
Kim H., Lee H. W., Myung Y. S., 2006, Phys. Lett. B, 632, 605
Kritpetch C., Muhammad C., Gumjudpai B., 2020, Phys. Dark Univ., 30, 100712
Leon G., Magaña J., Hernández-Almada A., García-Aspeitia M. A., Verdugo T., Motta V., 2021, J. Cosmol. Astropart. Phys., 2021, 032
Li M., 2004, Phys. Lett. B, 603, 1
Li X., Shafieloo A., 2019, ApJ, 883, L3
Li X., Shafieloo A., 2020, ApJ, 902, 58
Li M., Li X.-D., Wang S., Zhang X., 2009, J. Cosmol. Astropart. Phys., 06, 036
Lin C., 2021, J. Cosmol. Astropart. Phys., 2021, 003
Lu J., Saridakis E. N., Setare M. R., Xu L., 2010, J. Cosmol. Astropart. Phys., 03, 031
Lymperis A., Basilakos S., Saridakis E. N., 2021, Eur. Phys. J. C, 81, 1037
Maartens R., Koyama K., 2010, Living Rev. Relativ., 13, 5
Magaña J., Amante M. H., García-Aspeitia M. A., Motta V., 2018, MNRAS, 476, 1036
Mamon A. A., Paliathanasis A., Saha S., 2021, Eur. Phys. J. Plus, 136, 134
Micheletti S. M. R., 2010, J. Cosmol. Astropart. Phys., 05, 009
Moradpour H., Ziaie A. H., Kord Zangeneh M., 2020, Eur. Phys. J. C, 80, 732
Moresco M. et al., 2016, J. Cosmol. Astropart. Phys., 1605, 014
Motta V., García-Aspeitia M. A., Hernández-Almada A., Magaña J., Verdugo T., 2021, Universe, 7, 163
Nadathur S., Percival W. J., Beutler F., Winther H., 2020, Phys. Rev. Lett., 124, 221301
Nojiri S., Odintsov S. D., 2006, Gen. Relativ. Gravity, 38, 1285
Nojiri S., Odintsov S. D., 2017, Eur. Phys. J. C, 77, 528
Nojiri S., Odintsov S. D., Paul T., 2021, Symmetry, 13, 928
Nunes R. C., Yadav S. K., Jesus J. F., Bernui A., 2020, MNRAS, 497, 2133
Pan S., Yang W., Di Valentino E., Shafieloo A., Chakraborty S., 2019, J. Cosmol. Astropart. Phys., 06, 062
Pavon D., Zimdahl W., 2005, Phys. Lett. B, 628, 206
Perko L., 2000, Differential Equations and Dynamical Systems, 3rd edn. Springer, New York
Perlmutter S., Aldering G., Goldhaber G., Knop R. A., Nugent P., others Project T. S. C., 1999, ApJ, 517, 565
Riess A. G. et al., 1998, AJ, 116, 1009
Riess A. G., Casertano S., Yuan W., Macri L. M., Scolnic D., 2019, ApJ, 876, 85
Riess A. G., Casertano S., Yuan W., Bowers J. B., Macri L., Zinn J. C., Scolnic D., 2021, ApJ, 908, L6
Saridakis E. N. et al., 2021, Modified Gravity and Cosmology: An Update by the CANTATA Network. preprint (arXiv:2105.12582)
Saridakis E. N., 2008a, J. Cosmol. Astropart. Phys., 04, 020
Saridakis E. N., 2008b, Phys. Lett. B, 660, 138
Saridakis E. N., 2018, Phys. Rev. D, 97, 064035
Saridakis E. N., 2020, Phys. Rev. D, 102, 123525
Saridakis E. N., Basilakos S., 2021, Eur. Phys. J. C, 81, 7
Saridakis E. N., Bamba K., Myrzakulov R., Anagnostopoulos F. K., 2018, J. Cosmol. Astropart. Phys., 12, 012
Schwarz G., 1978, Ann. Statist., 6, 461
Scolnic D. M. et al., 2018, ApJ, 859, 101
Setare M. R., Saridakis E. N., 2008, Phys. Lett. B, 670, 1
Setare M. R., Saridakis E. N., 2009, Phys. Lett. B, 671, 331
Setare M. R., Vagenas E. C., 2008, Phys. Lett. B, 666, 111
Shah P., Lemos P., Lahav O., 2021, Astronomy and Astrophysics Review, 29, 9
Shajib A. J. et al., 2020, MNRAS, 494, 6072
Shekh S. H., 2021, Phys. Dark Univ., 33, 100850
Spergel D. N. et al., 2003, ApJS, 148, 175
Sugiura N., 1978, Commun. Stat. - Theory Methods, 7, 13
Susskind L., 1995, J. Math. Phys., 36, 6377
Suwa M., Nihei T., 2010, Phys. Rev. D, 81, 023519
Villanueva J., 2015, J. Cosmol. Astropart. Phys., 2015, 045
Wainwright J., Ellis G. F. R., 1997, Dynamical Systems in Cosmology. Cambridge University Press, Cambridge
Wang B., Gong Y.-g., Abdalla E., 2005, Phys. Lett. B, 624, 141
Wang S., Wang Y., Li M., 2017, Phys. Rep., 696, 1
Weinberg S., 1989, Rev. Mod. Phys., 61, 1
Zel'dovich Y., Krasinski A., Zeldovich Y., 1968, Sov. Phys. Usp., 11, 381
Zhang X., 2009, Phys. Rev. D, 79, 103509
Zhang X., Wu F.-Q., 2005, Phys. Rev. D, 72, 043524
't Hooft G., 1993, Zeitschrift für Physik A: Hadrons and Nuclei, Vol. 349. p. 241

This paper has been typeset from a TEX/LATEX file prepared by the author.